Neurobiology of Disease

# Phases of Hyperconnectivity and Hypoconnectivity in the Default Mode and Salience Networks Track with Amyloid and Tau in Clinically Normal Individuals

**Aaron P. Schultz,[1,5] Jasmeer P. Chhatwal,[1,5] Trey Hedden,[2,5] Elizabeth C. Mormino,[1,5] Bernard J. Hanseeuw,[1,2] Jorge Sepulcre,[2] Willem Huijbers,[1,8] Molly LaPoint,[1] Rachel F. Buckley,[1,6,7] Keith A. Johnson,[2,3] and Reisa A. Sperling[1,4]**

Departments of [1]Neurology and [2]Radiology, and [3]Division of Nuclear Medicine and Molecular Imaging, Department of Radiology, Massachusetts General Hospital, Harvard Medical School, Boston, Massachusetts 02114, [4]Center for Alzheimer Research and Treatment, Department of Neurology, Brigham and Women's Hospital, Harvard Medical School, Boston, Massachusetts 02115, [5]Athinoula A. Martinos Center for Biomedical Imaging, Department of Radiology, Massachusetts General Hospital, Charlestown HealthCare Center, Charlestown, Massachusetts 02129, [6]Florey Institute of Neuroscience and Mental Health, Parkville 3052, Victoria, Australia, and [7]Melbourne School of Psychological Sciences, University of Melbourne, Melbourne 3010, Victoria, Australia, and [8]Jheronimus Academy of Data Science, Cognitive Science and Artificial Intelligence, Tilburg University, 5211 DA, 's-Hertogenbosch, The Netherlands

**Alzheimer's disease (AD) is characterized by two hallmark molecular pathologies: amyloid a$\beta_{1-42}$ and Tau neurofibrillary tangles. To date, studies of functional connectivity MRI (fcMRI) in individuals with preclinical AD have relied on associations with *in vivo* measures of amyloid pathology. With the recent advent of *in vivo* Tau-PET tracers it is now possible to extend investigations on fcMRI in a sample of cognitively normal elderly humans to regional measures of Tau. We modeled fcMRI measures across four major cortical association networks [default-mode network (DMN), salience network (SAL), dorsal attention network, and frontoparietal control network] as a function of global cortical amyloid [Pittsburgh Compound B (PiB)-PET] and regional Tau (AV1451-PET) in entorhinal, inferior temporal (IT), and inferior parietal cortex. Results showed that the interaction term between PiB and IT AV1451 was significantly associated with connectivity in the DMN and salience. The interaction revealed that amyloid-positive (a$\beta^+$) individuals show increased connectivity in the DMN and salience when neocortical Tau levels are low, whereas a$\beta^+$ individuals demonstrate decreased connectivity in these networks as a function of elevated Tau-PET signal. This pattern suggests a hyperconnectivity phase followed by a hypoconnectivity phase in the course of preclinical AD.**

*Key words:* amyloid; AV1451; DMN; fcMRI; PiB; Tau

**Significance Statement**

**This article offers a first look at the relationship between Tau-PET imaging with $F^{18}$-AV1451 and functional connectivity MRI (fcMRI) in the context of amyloid-PET imaging. The results suggest a nonlinear relationship between fcMRI and both Tau-PET and amyloid-PET imaging. The pattern supports recent conjecture that the AD fcMRI trajectory is characterized by periods of both hyperconnectivity and hypoconnectivity. Furthermore, this nonlinear pattern can account for the sometimes conflicting reports of associations between amyloid and fcMRI in individuals with preclinical Alzheimer's disease.**

## Introduction

By measuring the coordination of time-varying brain activity, functional connectivity magnetic resonance imaging (fcMRI) can be a sensitive indicator of early network disruption and may prove useful in tracking the progression of neurodegenerative diseases. fcMRI has been studied previously in Alzheimer's disease (AD) across a range of asymptomatic and symptomatic clinical states. It has been well established that, relative to clinically

Received Oct. 17, 2016; revised March 7, 2017; accepted March 8, 2017.

Author contributions: A.P.S., K.A.J., and R.S. designed research; A.P.S., J.P.C., T.H., B.J.H., M.L., K.A.J., and R.A.S. performed research; A.P.S., J.P.C., E.C.M., J.S., W.H., R.F.B., K.A.J., and R.A.S. analyzed data; A.P.S., J.P.C., T.H., E.C.M., B.J.H., J.S., W.H., M.L., R.F.B., K.A.J., and R.A.S. wrote the paper.

This work was supported in part by shared instrumentation grants and Grants S10OD010364, S10RR023401, and 1S10RR019307–01 from the Martinos Center for Biomedical Imaging. The research was also supported in major part by Harvard Aging Brain Study Grant P01-AG-036694. T.H. received funding from National Institutes of Health (NIH) Grants K01-AG-040197, P01-AG-036694, P50-AG-005134, R01-AG-053509, and R01-AG-034556. E.C.M. received funding from NIH Grant K01-AG-051718. B.J.H. received support from the Belgian American Education Foundation. J.S. received funding from HIH Grant K23EB019023. R.F.B. received funding from the Australian National Health and Medical Research Council and Australian Research Council Dementia Research Fellowship APP1105576. K.A.J. received funding from NIH Grants R01-EB-014894, R21-AG-038994, R01-AG-026484, R01-AG-034556, P50-AG-00513421, U19-AG-10483, P01-AG-036694, R13-AG-042201174210, R01-AG-027435, and R01-AG-037497; and

normal (CN) control subjects, patients with a clinical diagnosis of AD exhibit widespread differences in functional connectivity across multiple cortical networks (Damoiseaux et al., 2012; Wang et al., 2007; Petrella et al., 2011; Brier et al., 2012; Chhatwal et al., 2013; Jack et al., 2013; Schultz et al., 2014; Jones et al., 2016). Even at the stage of mild cognitive impairment (MCI), there are notable differences compared with CN control subjects, and these differences are accentuated when the analysis is focused on MCI who progress to dementia (Petrella et al., 2011).

The relationship between early AD pathology and fcMRI is more tenuous in preclinical (asymptomatic) AD (Sperling et al., 2011), where consensus in terms of location, size, and direction of fcMRI effects has been more difficult to establish. While many studies have reported decreased functional connectivity with increased amyloid (a$\beta$) burden in the medial temporal lobe (MTL), posterior midline, and parietal regions (Hedden et al., 2009; Sheline et al., 2010a; Chhatwal et al., 2013; Wang et al., 2013; Brier et al., 2014), other studies have reported regions of both increased and decreased connectivity with elevated amyloid (Mormino et al., 2011; Lim et al., 2014). One account of these discrepant reports is that there are both hyperconnectivity and hypoconnectivity effects at different points in the preclinical AD spectrum. Using longitudinal amyloid-PET imaging, Jack et al. (2013) categorized individuals according to changes in amyloid burden and reported increased posterior DMN connectivity among low amyloid (a$\beta^-$) individuals who became a$\beta^+$ at follow-up, whereas patients with AD dementia had reduced connectivity, suggesting both hyperconnectivity and hypoconnectivity effects at different stages of disease.

The focus of these fcMRI studies in preclinical AD have largely been on amyloid status. The opportunity to examine both hallmark AD molecular pathologies, in particular variations in regional Tau pathologic burden and/or interactions between regional Tau and amyloid burden, may provide insight into the nature of the effects of preclinical AD pathology on functional connectivity. With the recent advent of Tau-PET ligands, we now extend the study of fcMRI in the context of preclinical AD to PET measures of amyloid and regional Tau burden obtained with Pittsburgh Compound B (PiB) and AV1451, respectively.

Prior reports on the relationship between amyloid-PET imaging and Tau-PET imaging (Villemagne et al., 2015; Cho et al., 2016; Johnson et al., 2016; Schöll et al., 2016; Sepulcre et al., 2016) have revealed highly significant associations between cortical amyloid-PET and AV1451 signals in regions associated with Braak stages (Braak et al., 2006, 2011). Notably, a pattern of MTL [entorhinal (ET)/parahippocampal], fusiform, inferior temporal (IT), parietal, and posterior midline regions define the standard AD-type pattern of paired helical filament (PHF) Tau as measured by AV1451. In preclinical AD cohorts, this pattern is generally limited to MTL, fusiform, and inferior temporal regions and is generally lower than MCI/AD cohorts, with few cases of elevated signal outside these regions. Also of interest, low-amyloid subjects also have elevated AV1451 signaling in medial and lateral temporal regions, although it is of smaller magnitude than in high-amyloid subjects. This suggests that some degree of Tau pathology outside the MTL is present independent of amyloid. We hypothesized that entorhinal and inferior temporal regions would be good indicators of nascent AD-related Tau pathology, and the inferior parietal (IP) region was used as a check against the possibility of relevant low-level AV1451 signal associated with more advanced Braak stages.

## Materials and Methods

*Participants.* Ninety-one participants from the Harvard Aging Brain Study (Grant P01-AG036694) with AV1451-PET, PiB-PET, and resting-state fMRI (rsfMRI) collected within 1 year were included in the present study (MR vs PiB = 110 ± 72 d; MR vs AV1451 = 129 ± 82 d; PiB vs AV1451 = 81 ± 74 d). All participants were clinically normal at baseline and at the assessment closest to the AV1451 scan. This classification was determined by a Clinical Dementia Rating of 0 (Morris, 1993), a Geriatric Depression Scale score of <11 (Yesavage et al., 1982), a Mini Mental State Examination score of >25 (Folstein et al., 1975), and performance within education-adjusted norms for Logical Memory Story A delayed recall (Wechsler, 1987). All study procedures were approved by the Partners Healthcare institutional review board, and all participants provided written informed consent.

The sample consisted of 54 females and 37 males, with a mean age of 75.78 ± 6.14 years having 15.69 ± 2.95 years of education. Thirty-two participants were APOE$\varepsilon$4 carriers, and 30 participants were categorized as amyloid positive using a quantitative threshold (20 of whom were $\varepsilon$4 carriers).

*Resting-state fMRI.* All data were collected on two matched 3T Trio Tim scanners (Siemens Medical Systems) using 12-channel phased-array head coils at the Athinoula A. Martinos Center for biomedical imaging in Charlestown, MA. Scanner noise was attenuated using foam earplugs. fcMRI data were acquired using a gradient-echo echoplanar imaging sequence sensitive to BOLD contrast. Whole-brain coverage, including the cerebellum, was acquired aligned parallel to the anterior/posterior commissure using the following parameters: repetition time (TR), 3000 ms; echo time (TE), 30 ms, flip angle, 85°; field of view, 216 × 216 mm; matrix, 72 × 72; and 3 × 3 × 3 mm voxels; 124 volumes were acquired in each of two 6 and 12 min runs (including 4 dummy volumes; 12 s). Instructions were to lie still, remain awake, and keep eyes open.

All resting-state data were processed using SPM8 (http://www.fil.ion.ucl.ac.uk/spm/). The first four volumes of each run were excluded to allow for T1 equilibration. Each run was slice time corrected, realigned to the first volume of each run with INRIAlign (http://www-sop.inria.fr/epidaure/software/INRIAlign/; Freire and Mangin, 2001), normalized to the MNI 152 EPI template (Montreal Neurological Institute, Montreal, Quebec, Canada), and smoothed with a 6 mm FWHM Gaussian kernel. Following these standard preprocessing steps, additional processing known to be beneficial for fcMRI analysis was conducted. These included the following (sequentially, and in this order): (1) regression of realignment parameters (plus first derivatives) to reduce movement artifacts on connectivity; and (2) temporal bandpass filtering (second-order Butterworth filter) to remove frequencies outside of the 0.01–0.08 Hz band.

Data were then processed with template-based rotation (TBR; Schultz et al., 2014), using the same template maps as published in the study by Schultz et al. [2014; TBR scripts and templates (nifti format) are available at http://mrtools.mgh.harvard.edu]. Whole-network measures for the default-mode network (DMN), salience (SAL) network (also called the ventral attention network), dorsal attention network (DAN), left fronto-parietal control network (FPCN), and right FPCN were extracted as

Alzheimer's Association Grant ZEN-10–174210. R.A.S. has received research support from NIH Grants P01-AG-036694, U01-AG-032438, U01-AG-024904, R01-AG-037497, R01-AG-034556, K24-AG-035007, P50-AG-005134, U19-AG-010483, and R01-AG027435; Fidelity Biosciences; the Harvard NeuroDiscovery Center; and the Alzheimer's Association.

A.P.S. has been a paid consultant for Janssen Pharmaceuticals and Biogen. E.C.M. has served as a consultant for Biogen and has received research support from Eli Lilly and Janssen Pharmaceuticals. K.A.J. has served as paid consultant for Bayer, GE Healthcare, Janssen Alzheimer's Immunotherapy, Siemens Medical Solutions, Genzyme, Novartis, Biogen, Roche, ISIS Pharma, AZTherapy, GEHC, Lundberg, and Abbvie; is a site coinvestigator for Lilly/Avid, Pfizer, Janssen Immunotherapy, and Navidea; and has spoken at symposia sponsored by Janssen Alzheimer's Immunotherapy, and Pfizer. R.A.S. has served as a paid consultant for Abbvie, Biogen, Bracket, Genentech, Lundbeck, Roche, and Sanofi; has served as a coinvestigator for Avid, Eli Lilly, and Janssen Alzheimer Immunotherapy clinical trials; has spoken at symposia sponsored by Eli Lilly, Biogen, and Janssen; and has received research support from Janssen Pharmaceuticals and Eli Lilly (these relationships are not related to the content in the manuscript). The authors declare no other competing financial interests.

Correspondence should be addressed to Dr. Reisa A. Sperling, Center for Alzheimer Research and Treatment, Department of Neurology, Brigham and Women's Hospital, Harvard Medical School, 221 Longwood Avenue, Boston, MA 02115. E-mail: reisa@bwh.harvard.edu.

DOI:10.1523/JNEUROSCI.3263-16.2017

described by Schultz et al. (2014). This included averaging all values within a mask defined on the template maps at >40% of the maximum value in the corresponding template map. Since DMN and salience were represented in a single map as anticorrelated networks, the salience was defined as <40% of the minimum value.

As an additional step [for seed-based region of interest (ROI) analyses only], we regressed out the average signal from white matter, ventricles, and global signal (plus first derivatives; Vincent et al., 2006; Van Dijk et al., 2010). Note that the operations were conducted in the specified order to prevent the reintroduction of nuisance variance in the stop-band frequencies (Hallquist et al., 2013). While white matter, ventricle, and global signal were regressed after bandpass filtering, the signals were taken from the bandpass-filtered data and so did not inadvertently reintroduce nuisance variance outside of the stop band. For seed-based analyses, we used a set of cluster-based seed regions defined on the template maps across the same networks as described above. Additional details can be found in the study by Shaw et al. (2015); and seed masks for each ROI can be found on-line at http://mrtools.mgh.harvard.edu/index.php?title=Downloads.

*Structural MRI.* Structural T1-weighted images were acquired as magnetization-prepared rapid acquisition gradient echo with the following acquisition parameters: TR, 2300; TE, 2.95; TI, 900 ms; flip angle, 9°; resolution, 1.1 × 1.1 × 1.2 mm; acceleration (GRAPPA), 2×. Notably, this is the same acquisition used in ADNI2-GO.

The structural MRI data were processed with Freesurfer version 5.1 (http://surfer.nmr.mgh.harvard.edu; Dale et al., 1999) and were automatically parcellated using the Desikan-Killany atlas (Desikan et al., 2006) for cortical ROIs, and the Freesurfer ASEG atlas (Fischl et al., 2002) for subcortical ROIs. Freesurfer-automated segmentation results were manually evaluated to ensure the accuracy of the results (for additional details, see https://www.nmr.mgh.harvard.edu/lab/harvardagingbrain/tools).

*PET imaging.* $^{11}$C Pittsburgh Compound B was prepared and PET data were acquired as described previously (Sperling et al., 2009). $^{11}$C PiB PET was acquired with an 8.5–15 mCi bolus injection followed immediately by a 60 min dynamic acquisition in 69 frames (12 × 15 s, 57 × 60 s).

$^{18}$F AV1451 was prepared at Massachusetts General Hospital with a mean radiochemical yield of 14 ± 3% and specific activity of 216 ± 60 GBq/μmol (5837 ± 1621 mCi/μmol) at the end of synthesis (60 min) and validated for human use (Shoup et al., 2013). Images were acquired from 80 to 100 min in 4 × 5 min frames after a 10.0 ± 1.0 mCi bolus injection.

All PET data were acquired using a Siemens/CTI ECAT HR+ Scanner (3D mode; 63 image planes; 15.2 cm axial field of view; 5.6 mm transaxial resolution; 2.4 mm slice interval). PET data were reconstructed, attenuation corrected, and evaluated to verify adequate count statistics and the absence of head motion.

PET images were coregistered to the corresponding T1 image for each subject using a 6 dof rigid-body registration and structural ROIs, as determined by Freesurfer, were mapped into native PET space. For both PiB and AV1451, we used a cerebellar gray matter reference region from the Freesurfer aseg atlas, as previously described (Becker et al., 2011; Chien et al., 2013; Johnson et al., 2016), with AV1451 measures computed as standardized uptake value ratios (SUVRs) from the 80–100 min time frame and PiB measures computed as distribution volume ratios (DVRs) using the Logan graphical method (Logan et al., 1990), with slopes extracted from the 40–60 min time frame.

Additionally, we performed partial volume correction (PVC) using the geometric transform matrix method (Labbe et al., 1998; Rousset et al., 1998), as implemented in Freesurfer 6.0 and described by Greve et al. (2016), using a slightly modified Freesurfer atlas mapped to each participants native structural space that included ROIs for CSF, white matter, and extracerebral structures. The PVC processing was performed assuming a uniform 6 mm point spread function.

Based on prior studies we used a single PiB measure of global cortical amyloid burden from regions including the following: bilateral precuneus, rostral anterior cingulate, medial orbito-frontal, superior frontal, rostral middle frontal, inferior parietal, inferior temporal, and middle temporal (simple mean across ROI values), the so-called frontal, lateral, retrosplenial ROI (Mormino et al., 2014b). PiB measures were used both continuously and dichotomously. The threshold for dichotomization into high- and low-amyloid groups was 1.2 and was derived via a Gaussian mixture model as described by Mormino et al. (2014a).

For AV1451, we focused our analyses on three structurally defined regions of interest: entorhinal (ET), inferior temporal (IT), and inferior parietal (IP). Entorhinal cortex was chosen as it is among the first areas to develop Tau pathology, even in the absence of amyloid. IT cortex was used as the current best choice of a surrogate marker of early AD related Tau spread into neocortex (IT AV1451 showed the largest effect size between impaired and nonimpaired individuals as reported by Johnson et al. (2016). The IP area was chosen as a marker of additional spread of Tau pathology into other regions of cortex that are associated with more advanced Braak stages.

*Whole-network analysis.* We investigated the relationship between each fcMRI network measure and PiB-PET and AV1451-PET controlling for age, sex, average movement (mean movement as measured by the Euclidean distance between volumes) during the rsfMRI scan, the temporal signal-to-noise ratio measured from the rsfMRI scan, and the scanner (two matched Siemens Trio Tim scanners were used for data collection). For each network, we investigated the following hierarchical set of models: (1) fcMRI ~ PiB + covariates; (2) fcMRI ~ AV1451 + covariates; (3) fcMRI ~ PiB + AV1451 + covariates; (4) fcMRI ~ PiB × AV1451 + covariates; and (5) fcMRI ~ PiB group × AV1451 + covariates.

This set of models was designed to look at interactions between measures of amyloid and Tau pathology, as well as the main effects of each molecular marker in the context of collinearity between PiB and AV1451 measures. PiB was also used dichotomously (PiB group) using our previously published threshold of 1.2 DVR units (Mormino et al., 2014b). To help curb the effects of positive skew in both the PiB and AV1451 distributions, both measures were log transformed before being entered into the models (effects were similar with and without log transforms).

*Node-based connectivity analysis.* To investigate the possibility of effects localized to particular nodes within a network or effects involving internodal connectivity between networks, we performed a separate exploratory analysis in which each network was broken into a set of constituent nodes (29 nodes across the networks analyzed). Time-series data for each node were extracted from the rsfMRI scans, and a node-to-node connectivity measurement for each pair of nodes was made for each subject. We then ran the models listed above for each node-to-node connection to evaluate localized effects of amyloid and Tau. Data were then visualized using a schema-ball plot (mrtools.mgh.harvard.edu), where the corresponding statistic for each connection is visualized as a color-graded line between the corresponding nodes. This resulted in a visualization that represents the sensitivity of node-to-node connectivity to the effect of interest. Additional details can be found in the study by Shaw et al. (2015, supplemental data). We also separated the connections into positive and negative connections based on the mean connectivity between nodes in the sample, and then reverse scored anti-correlations so that higher values in both sets represent connectivity strengths further from 0.

## Results

### Relationships between and among PET measures

Similar to our previous report examining AV1451 Tau PET across the spectrum of AD (Johnson et al., 2016), there was a significant correlation between the cortical aggregate PiB-PET measure and regional AV1451 measures. In the present sample, we observed significant correlations with PiB-PET for all three AV1451 regions explored in the current study, as follows: ET ($r = 0.46$; $p < 0.001$); IT ($r = 0.40$; $p < 0.001$), and IP ($r = 0.31$; $p = 0.003$). The AV1451 measures from the three ROIs were significantly correlated with one another, as follows: ET by IT ($r = 0.69$; $p \ll 0.001$); ET by IP ($r = 0.54$; $p \ll 0.001$); and IT by IP (0.71; $p \ll 0.001$). As with previous reports (Johnson et al., 2016; Sepulcre et al., 2016), the PiB groups showed significant differences

**Table 1. Summary of results from statistical models**

| | Models 1 and 2 | | Model 3 | | Model 4 | Model 5 |
|---|---|---|---|---|---|---|
| | PiB | Tau | PiB | Tau | PiB × Tau | PG × Tau |
| Entorhinal AV1451 | | | | | | |
| DMN | $t_{(84)} = 1.086; p = 0.28$ | $t_{(84)} = 0.150; p = 0.88$ | $t_{(83)} = 1.127; p = 0.26$ | $t_{(83)} = -0.355; p = 0.72$ | $t_{(82)} = -0.226; p = 0.82$ | $t_{(82)} = 0.628; p = 0.53$ |
| Salience | $t_{(84)} = 0.478; p = 0.63$ | $t_{(84)} = -0.770; p = 0.44$ | $t_{(83)} = 0.902; p = 0.37$ | $t_{(83)} = -1.084; p = 0.28$ | $t_{(82)} = -0.959; p = 0.34$ | $t_{(82)} = -0.110; p = 0.91$ |
| DAN | $t_{(84)} = 0.601; p = 0.55$ | $t_{(84)} = 0.444; p = 0.66$ | $t_{(83)} = 0.451; p = 0.65$ | $t_{(83)} = 0.202; p = 0.84$ | $t_{(82)} = 0.515; p = 0.61$ | $t_{(82)} = 0.998; p = 0.32$ |
| Left FPCN | $t_{(84)} = 1.596; p = 0.11$ | $t_{(84)} = 1.734; p = 0.09$ | $t_{(83)} = 0.939; p = 0.35$ | $t_{(83)} = 1.153; p = 0.25$ | $t_{(82)} = 0.803; p = 0.42$ | $t_{(82)} = 1.673; p = 0.10$ |
| Right FPCN | $t_{(84)} = 0.501; p = 0.62$ | $t_{(84)} = 0.951; p = 0.34$ | $t_{(83)} = 0.099; p = 0.92$ | $t_{(83)} = 0.809; p = 0.42$ | $t_{(82)} = -1.080; p = 0.28$ | $t_{(82)} = -0.704; p = 0.48$ |
| Inferior temporal AV1451 | | | | | | |
| DMN | $t_{(84)} = 1.086; p = 0.28$ | $t_{(84)} = -0.141; p = 0.89$ | $t_{(83)} = 1.197; p = 0.23$ | $t_{(83)} = -0.531; p = 0.60$ | ***$t_{(82)} = -3.616; p = 0.00$*** | ***$t_{(82)} = -2.494; p = 0.01$*** |
| Salience | $t_{(84)} = 0.478; p = 0.63$ | $t_{(84)} = -1.308; p = 0.19$ | $t_{(83)} = 0.972; p = 0.33$ | $t_{(83)} = -1.557; p = 0.12$ | ***$t_{(82)} = -4.774; p = 0.00$*** | ***$t_{(82)} = -3.642; p = 0.00$*** |
| DAN | $t_{(84)} = 0.601; p = 0.55$ | $t_{(84)} = -0.880; p = 0.38$ | $t_{(83)} = 0.949; p = 0.35$ | $t_{(83)} = -1.145; p = 0.26$ | $t_{(82)} = -1.224; p = 0.22$ | $t_{(82)} = -1.073; p = 0.29$ |
| Left FPCN | $t_{(84)} = 1.596; p = 0.11$ | $t_{(84)} = 0.601; p = 0.55$ | $t_{(83)} = 1.468; p = 0.15$ | $t_{(83)} = 0.083; p = 0.93$ | $t_{(82)} = -1.184; p = 0.24$ | $t_{(82)} = -0.959; p = 0.34$ |
| Right FPCN | $t_{(84)} = 0.501; p = 0.62$ | $t_{(84)} = -0.133; p = 0.89$ | $t_{(83)} = 0.575; p = 0.57$ | $t_{(83)} = -0.316; p = 0.75$ | ***$t_{(82)} = -2.237; p = 0.03$*** | ***$t_{(82)} = -2.293; p = 0.02$*** |
| Inferior parietal AV1451 | | | | | | |
| DMN | $t_{(84)} = 1.086; p = 0.28$ | $t_{(84)} = 0.557; p = 0.58$ | $t_{(83)} = 0.960; p = 0.34$ | $t_{(83)} = 0.255; p = 0.80$ | ***$t_{(82)} = -1.890; p = 0.06$*** | $t_{(82)} = -1.450; p = 0.15$ |
| Salience | $t_{(84)} = 0.478; p = 0.63$ | $t_{(84)} = -0.381; p = 0.70$ | $t_{(83)} = 0.612; p = 0.54$ | $t_{(83)} = -0.540; p = 0.59$ | ***$t_{(82)} = -2.668; p = 0.01$*** | ***$t_{(82)} = -2.369; p = 0.02$*** |
| DAN | $t_{(84)} = 0.601; p = 0.55$ | $t_{(84)} = -0.149; p = 0.88$ | $t_{(83)} = 0.670; p = 0.50$ | $t_{(83)} = -0.337; p = 0.74$ | $t_{(82)} = -1.010; p = 0.32$ | $t_{(82)} = -0.982; p = 0.33$ |
| Left FPCN | $t_{(84)} = 1.596; p = 0.11$ | $t_{(84)} = 0.594; p = 0.55$ | $t_{(83)} = 1.476; p = 0.14$ | $t_{(83)} = 0.145; p = 0.89$ | $t_{(82)} = -0.834; p = 0.41$ | $t_{(82)} = -0.466; p = 0.64$ |
| Right FPCN | $t_{(84)} = 0.501; p = 0.62$ | $t_{(84)} = -0.034; p = 0.97$ | $t_{(83)} = 0.530; p = 0.60$ | $t_{(83)} = -0.186; p = 0.85$ | ***$t_{(82)} = -1.968; p = 0.05$*** | $t_{(82)} = -1.777; p = 0.08$ |

Robust effects are limited to amyloid by inferior temporal (IT) AV1451 interactions for the DMN and Salience networks. Of note, the main effects outside of the context of the interaction term are nonsignificant. Effects highlighted with bold/italicized font survive FWE of $p < 0.0033$ (0.05/15 tests); effects highlighted with bold font are significant at an uncorrected $p$ value of $<0.05$. Results for IT AV1451 in DMN and Salience networks are present when using PiB continuously or dichotomously using PiB group (PG).

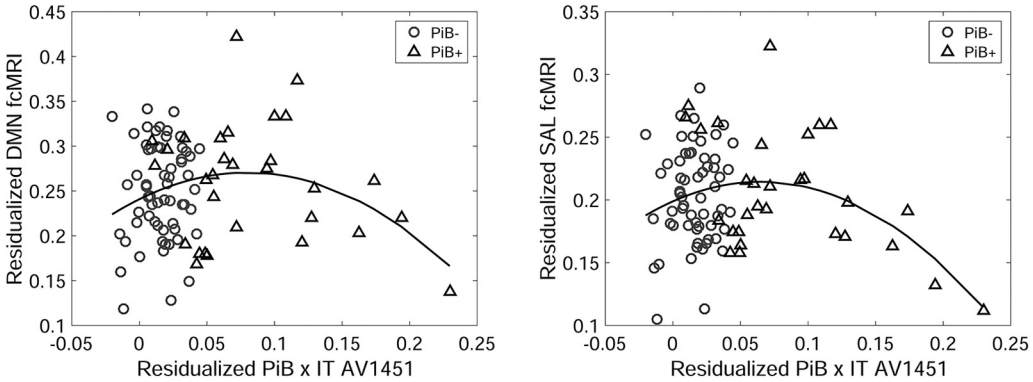


**Figure 1.** Visualization of the PiB × IT AV1451 interaction term vs DMN connectivity (left) and salience (SAL) connectivity (right). Both networks show a significant quadratic pattern that can be described as a positive relationship with amyloid when the IT AV1451 signal is low and as a negative association with the IT AV1451 signal when the PiB signal is high. The significant interaction is driven in large part by the relatively elevated connectivity seen in high-PiB low-IT AV1451 participants (triangular points near the middle of the *x*-axis).

using two-sample $t$ tests in entorhinal AV1451 ($t_{(89)} = 3.80$, $p < 0.001$), IT AV1451 ($t_{(89)} = 3.20$, $p = 0.002$), and IP AV1451 ($t_{(89)} = 2.01$, $p = 0.047$).

### Whole-network analyses

Results from the five models (see Materials and Methods) are reported in Table 1. We examined the relationship of AV1451 signal (in the ET, IT, and IP cortices) as well as the global amyloid burden to measures of functional connectivity in the following five cortical networks: the DMN, SAL, DAN, left FPCN, and right FPCN. Of note, we found the strongest effects using DMN and SAL with the interaction of PiB and AV1451 signal in IT cortex. No other effects survived correction for multiple comparisons (FWE for 15 tests, $p < 0.003$), although marginal effects were present for the interaction between inferior parietal Tau and PiB. We did not observe main effects outside the context of the interaction. For DMN connectivity, the PiB by inferior temporal AV1451 interaction term was significant both when PiB was tested continuously ($t_{(82)} = -3.616$; $p < 0.001$) and dichotomously ($t_{(82)} = -2.494$; $p = 0.010$). The same pattern was true of salience connectivity for continuous PiB ($t_{(82)} = -4.774$; $p < 0.001$) and dichotomous PiB ($t_{(82)} = -3.642$; $p < 0.001$). Statistical results for all five models are shown in Table 1.

Figure 1 depicts the results of the continuous interaction term (PiB × IT AV1451). Here the interaction term is well described as a quadratic, suggesting hyperconnectivity associated with elevated amyloid among participants with low IT AV1451 signal, followed by hypoconnectivity with an increasing IT AV1451 signal in individuals with higher amyloid levels. Figure 1 also shows that the vast majority of values on the low end of the interaction term are PiB -participants. Additionally, the inverted U shape of the fit explains the lack of main effects for PiB and AV1451.

To more thoroughly explore the significant interaction between PiB and IT AV1451, we examined the pattern within the high-PiB group only ($N = 30$). This analysis shows a linear relationship between increasing AV1451 signal in the inferior temporal cortex and decreasing functional connectivity in the DMN (partial $r = -0.42$, $p = 0.037$) and salience (partial $r = -0.67$; $p < 0.001$) networks. Examination within the low-PIB group ($N = 61$) showed weak positive relationships between functional connectivity and IT AV1451 in the DMN (partial $r = 0.28$, $p = 0.040$) and salience (partial $r = 0.29$, $p = 0.030$). Similarly, an analysis of PiB within a median split of IT AV1451 (IT Tau >< 1.18) shows a large effect of PiB in the low-Tau group ($N = 46$) for both DMN (partial $r = 0.44$, $p = 0.004$) and salience (partial $r = 0.45$, $p = 0.003$), whereas the effect of PiB in the high IT-

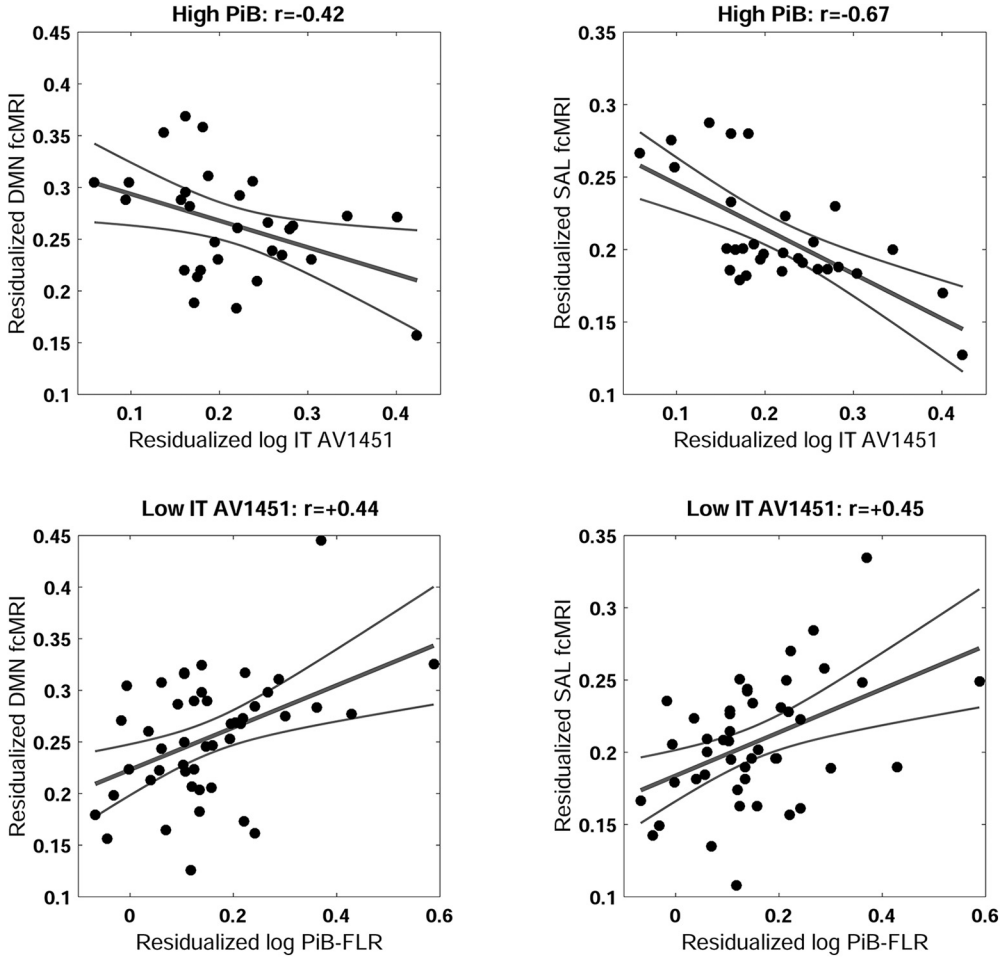


**Figure 2.** The top two panels show the relationship between inferior temporal (IT) AV1451 signal in the high PiB group (top) with DMN connectivity (left) and salience (SAL) connectivity (right). Within the context of high amyloid level, increased levels of IT AV1451 are associated with decreased connectivity in the DMN and SAL networks. The bottom two panels show the association between amyloid burden in the low-IT AV1451 signal subjects (median split) with DMN connectivity (left), and SAL (right). These two effects, the positive effect of amyloid when the IT AV1451 signal is low and the negative effect of IT AV1451 signal when amyloid level is high, account for the observed interaction effect and the absence of main effects.

AV1451 ($N = 45$) group was not significant for the DMN (partial $r = -0.14$, $p = 0.380$) and only marginally significant for the salience (partial $r = -0.27$, $p = 0.090$). This pattern of simple effects (Fig. 2) shows that the PiB by AV1451 interaction term in the full model is driven by the positive effect of PiB when IT AV1451 is relatively low, and the negative effect of IT AV1451 when PiB is high.

### Node-based connectivity analysis

Figure 3 depicts the statistical results for the PiB by IT AV1451 interaction term from model 4 on the node to node connections (406 pairs in total) thresholded at a liberal exploratory $p < 0.01$ uncorrected to reveal the global pattern of the effect. Lines outside the circle represent within-network connections, lines inside the circle represent between-network connections. The sign of the effects corresponds to whether the direction of the PiB × AV1451 interaction effect was related to increased connectivity (Fig. 3, yellow, away from 0 connectivity) or decreased connectivity (Fig. 3, purple, toward 0 connectivity). This analysis revealed that nearly all effects of decreasing connectivity are localized to the DMN and salience networks, providing additional support for the specificity of this effect to the DMN–salience axis. Of interest, the number of significant connections among salience nodes is smaller than observed for DMN and connections between DMN and salience nodes. This may indicate that the PiB by AV1451 interaction effect is most sensitive to the DMN–salience axis as a whole.

## Discussion

We examined the relationship between amyloid burden as measured by PiB-PET, PHF Tau burden as measured by AV1451-PET, and network integrity as measured by fcMRI in a sample of clinically normal elderly. The results point to an interaction between amyloid and regional PHF Tau in the IT cortex relating to fcMRI in the default mode and salience networks. Furthermore, the pattern of this interaction suggests a hyperconnectivity phase among a$\beta^+$ individuals who have low levels of AV1451 binding and a hypoconnectivity phase as IT Tau pathology accrues in the presence of elevated amyloid burden.

The amyloid cascade hypothesis in its most common formulation posits that amyloid accumulation precedes neocortical Tau accumulation and neurodegeneration (Hardy and Higgins, 1992). As such, molecular AD pathology can be described as a two-phase process of amyloid accumulation followed by continued amyloid accumulation and the spread of neurofibrillary tangles into neocortex. The results presented here suggest that these two periods of AD pathology have differential effects on functional connectivity, with the early amyloid accumulation phase

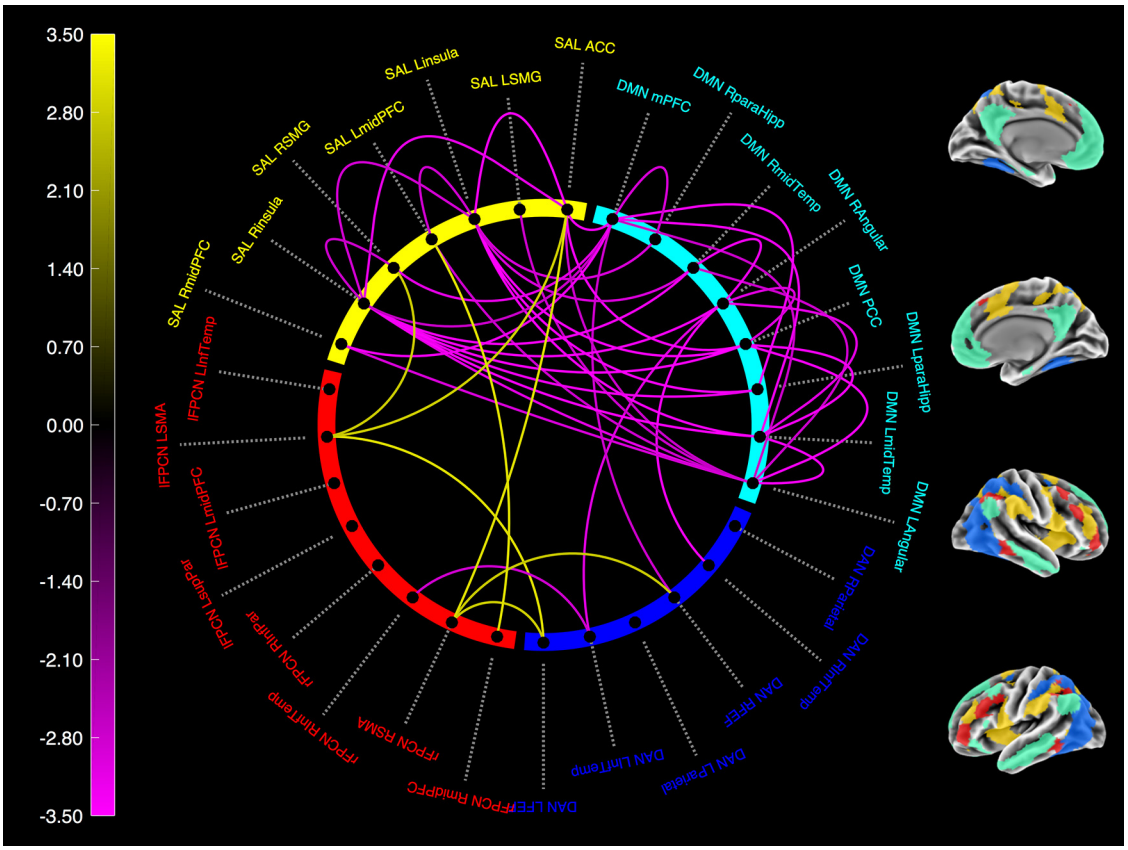


**Figure 3.** Node-level analysis of the IT AV1451 × PiB interaction term on connectivity between each pair of nodes. Lines on the outside of the figure correspond to within network connections. Lines on the inside correspond with between network connections. Purple colors represent decreased connectivity (movement toward 0); yellow colors represent increased connectivity (movement away from 0). Only connections with an effect of $p < 0.01$ are shown. The patterns of significant nodes correspond well to the whole-network analysis and demonstrate that the sensitivity to AV1451 and PiB is largely focused within and between the DMN and salience (SAL).

characterized by increased functional connectivity, followed by the progressive decline of functional connectivity with increased neocortical Tau pathology.

### Interpreting hyperconnectivity

While the effect of Tau in amyloid-positive individuals accords nicely with our expectations of decreased connectivity accompanying increased pathology, the evidence for increased connectivity with increased amyloid presents something of a puzzle when taken in the context of loss of connectivity later in the disease trajectory.

Evidence for a preclinical hyperconnectivity phase was reported in the study by Jack et al. (2013), where incident a$\beta$ positivity was cross-sectionally associated with increased posterior DMN connectivity. Increased functional connectivity has also been reported in individuals carrying the apolipoprotein $\varepsilon$4 (APOE$\varepsilon$4) risk allele for AD (Filippini et al., 2009; Sheline et al., 2010b; Westlye et al., 2011). APOE$\varepsilon$4 carriers have also been shown to have increased task-related activity during the performance of episodic memory tasks (Sperling et al., 2010; Huijbers et al., 2015; Oh et al., 2015, 2016). Hyperconnectivity has also been observed in psychiatric disorders such as schizophrenia and bipolar disorders (Whitfield-Gabrieli et al., 2009; Baker et al., 2014). Together, these findings indicate that hyperconnectivity likely has pathologic connotations.

From a more mechanistic perspective, hyperconnectivity may be an important component of a pathological feedback mechanism that is both being driven by and driving the production of amyloid and the accumulation of amyloid plaques (Busche and Konnerth, 2015). Recent studies have linked AD pathology with an increased incidence of late-onset seizure disorders and nonconvulsive epileptiform discharges (Palop and Mucke, 2009; Vossel et al., 2013; Born, 2015). In turn, nonconvulsive epileptiform activity has been linked to hypersynchronous neuronal activity (Khambhati et al., 2015). If correct, early amyloid-related hyperconnectivity would signify a disruption to the healthy functioning of large-scale neuronal networks.

There are alternative accounts for the observed pattern of results. First, it is possible that the effect we see is due to a survival bias such that high-amyloid individuals who are clinically normal are more likely to harbor a low Tau burden. The data from our laboratory and others suggest that individuals with high amyloid and high Tau burden are unlikely to remain clinically normal (Jack et al., 2016; Johnson et al., 2016). If increased connectivity is protective, one could easily imagine that within this group we are selecting for people with protective endophenotypes. These amyloid-resilient individuals could then be responsible for driving the interaction.

Second, increased connectivity may be compensatory and could represent a systems-level response to neuronal injury from pathological insult that allows for the maintenance of behavioral performance. This would result in a period of hyperactivity until the compensatory mechanisms are overwhelmed by neuronal loss, which would then lead to decreased connectivity.

Third, our interpretation of hyperconnectivity versus hypoconnectivity may be underdeveloped relative to the dynamic re-

ality of brain connectivity. For instance, a loss of functional dynamicity could result in the over-representation of specific brain activity states. This reduced dynamic flexibility would then manifest in our measures as increased connectivity in the "typical" brain states that form the basis of functional networks.

To explicate which of these models best characterizes the network disruption in preclinical AD will require cross-sectional replication of these results in other samples, longitudinal assessment of fcMRI data, and development of new analytic tools and functional sequences to more fully understand and measure the dynamic properties of connectivity.

### Interpreting hypoconnectivity

The hypoconnectivity effect is more straightforward, suggesting that the loss of functional connectivity—as with loss of structure and neuronal death—is more closely associated with neocortical Tau pathology than with amyloid. Notably, this suggests that the loss of connectivity is not directly caused by a$\beta$ toxicity but rather by Tau pathology, although a$\beta$ toxicity may impair the functioning of these networks, resulting in hyperconnectivity.

### Relationship to existing amyloid-fcMRI literature

Our present results also hold implications for prior studies of amyloid and APOE$\varepsilon$4 status with fcMRI data. Namely, the observed results are likely to be dependent on the specific makeup of the amyloid-positive group. If the amyloid-positive individuals are biased toward low Tau levels (e.g., young $\varepsilon$4 carriers), there may be an increased likelihood of observing hyperconnectivity effects. Conversely, if the amyloid-positive individuals in a given sample are biased toward elevated levels of neocortical Tau, then there likely will be a hypoconnectivity effect. If the amyloid-positive individuals are relatively balanced between low and elevated levels of Tau, then there may be no observable effect of amyloid. Thus, the pattern of hyperconnectivity followed by hypoconnectivity observed here may help to explain the varied effects reported in the literature, highlighting the need to consider additional pathologies beyond amyloid burden.

Additionally, given that there is a non-negligible AV1451 signal in low-amyloid subjects in both allocortical (i.e., entorhinal and parahippocampus) and neocortical (i.e., fusiform and inferior temporal) regions, it will be important to consider the effects of PHF-Tau on fcMRI in the absence of amyloid as it relates to generic aging processes and nonamyloid tauopathies.

A great deal of work remains to elucidate the relationship between fcMRI and preclinical AD pathology; however, it appears clear that *in vivo* Tau imaging will be critical to providing new insights into the sequence and consequences of the AD pathological cascade. One area of particular interest will be in discerning how propagation of Tau pathology is related to functional and structural network architecture. Recent work by Ossenkoppele et al. (2016) looking at clinically impaired AD variants found that spatial patterns of Tau pathology across AD phenotypes mirrored atrophy patterns and metabolic patterns, suggesting nonlocal spread of Tau, presumably via network connections. Recent work by Wu et al. (2016) demonstrated that neuronal activity can modulate the release of Tau, and that this Tau can spread through extracellular space, providing a potential mechanism for local spread of Tau pathology associated with hyperactivity. The extent to which the spread of nascent Tau pathology in preclinical populations mirrors functional network architecture remains to be elucidated.

### Interpreting default mode/salience effects

The observed effects were limited to default mode/salience network and were not observed in dorsal attention or control networks. Given the anticorrelated nature of the default mode/salience network in our dataset, observing the effect in both is not surprising and corresponds with previously reported functional connectivity effects across the AD spectrum (Brier et al., 2012). Furthermore, given the preclinical nature of this cohort, our findings support the hypothesis that the default-mode network is the first to be affected by nascent AD pathology, which is consistent with other reports (Hedden et al., 2009; Lim et al., 2014; Jones et al., 2016). Previous work in autosomal-dominant AD and APOE4 carriers have also implicated the DMN and salience networks in younger asymptomatic genetic at-risk individuals (Filippini et al., 2009; Machulda et al., 2011; Chhatwal et al., 2013).

AD is characterized by two primary molecular pathologies, both of which appear to be necessary for cognitive decline and progression to dementia (Vos et al., 2015). Amyloid-$\beta$ deposition begins in heteromodal cortices, largely overlapping the topology of the cortical connectivity hubs (Buckner et al., 2009), whereas Tau pathology accumulates early in the MTL, in regions strongly connected to cortical DMN regions (Ward et al., 2014). Moreover, episodic memory is typically the most salient cognitive symptom of early AD and relies on the interplay of DMN and MTL activity (Miller et al., 2008; Ward et al., 2015). Executive function also commonly declines in concert with episodic memory in aging and early AD, which may particularly implicate interplay between DMN network and salience networks (La Corte et al., 2016). Ongoing work in our group and others seeks to further differentiate the network alterations associated with aging and the earliest alterations specifically associated with the molecular pathologies of AD. These observations will guide the use of functional connectivity as an exploratory outcome measure in AD secondary prevention trials, aiming to decrease amyloid accumulation to prevent the spread of Tau pathology and cognitive decline associated with AD (Sperling et al., 2014).

## References

Baker JT, Holmes AJ, Masters GA, Yeo BT, Krienen F, Buckner RL, Öngür D (2014) Disruption of cortical association networks in schizophrenia and psychotic bipolar disorder. JAMA Psychiatry 71:109–118. CrossRef Medline

Becker JA, Hedden T, Carmasin J, Maye J, Rentz DM, Putcha D, Fischl B, Greve DN, Marshall GA, Salloway S, Marks D, Buckner RL, Sperling RA, Johnson KA (2011) Amyloid-$\beta$ associated cortical thinning in clinically normal elderly. Ann Neurol 69:1032–1042. CrossRef Medline

Born HA (2015) Seizures in Alzheimer's disease. Neuroscience 286:251–263. CrossRef Medline

Braak H, Alafuzoff I, Arzberger T, Kretzschmar H, Del Tredici K (2006) Staging of Alzheimer disease-associated neurofibrillary pathology using paraffin sections and immunocytochemistry. Acta Neuropathol 112:389–404. CrossRef Medline

Braak H, Thal DR, Ghebremedhin E, Del Tredici K (2011) Stages of the pathologic process in Alzheimer disease: age categories from 1 to 100 years. J Neuropathol Exp Neurol 70:960–969. CrossRef Medline

Brier MR, Thomas JB, Snyder AZ, Benzinger TL, Zhang D, Raichle ME, Holtzman DM, Morris JC, Ances BM (2012) Loss of intranetwork and internetwork resting state functional connections with Alzheimer's disease progression. J Neurosci 32:8890–8899. CrossRef Medline

Brier MR, Thomas JB, Fagan AM, Hassenstab J, Holtzman DM, Benzinger TL, Morris JC, Ances BM (2014) Functional connectivity and graph theory in preclinical Alzheimer's disease. Neurobiol Aging 35:757–768. CrossRef Medline

Buckner RL, Sepulcre J, Talukdar T, Krienen FM, Liu H, Hedden T, Andrews-Hanna JR, Sperling RA, Johnson KA (2009) Cortical hubs revealed by intrinsic functional connectivity: mapping, assessment of

stability, and relation to Alzheimer's disease. J Neurosci 29:1860–1873. CrossRef Medline

Busche MA, Konnerth A (2015) Neuronal hyperactivity—a key defect in Alzheimer's disease? Bioessays 37:624–632. CrossRef Medline

Chhatwal JP, Schultz AP, Johnson KA, Benzinger TLS, Jack C Jr, Ances BM, Sullivan CA, Salloway SP, Ringman JM, Koeppe RA, Marcus DS, Thompson P, Saykin AJ, Correia S, Schofield PR, Rowe CC, Fox NC, Brickman AM, Mayeux R, McDade E, et al (2013) Impaired default network functional connectivity in autosomal dominant Alzheimer disease. Neurology 81:736–744. CrossRef Medline

Chien DT, Bahri S, Szardenings AK, Walsh JC, Mu F, Su MY, Shankle WR, Elizarov A, Kolb HC (2013) Early clinical PET imaging results with the novel PHF-tau radioligand [F-18]-T807. J Alzheimers Dis 34:457–468. CrossRef Medline

Cho H, Choi JY, Hwang MS, Kim YJ, Lee HM, Lee HS, Lee JH, Ryu YH, Lee MS, Lyoo CH (2016) In vivo cortical spreading pattern of tau and amyloid in the Alzheimer disease spectrum. Ann Neurol 80:247–258. CrossRef Medline

Dale AM, Fischl B, Sereno MI (1999) Cortical surface-based analysis. I. Segmentation and surface reconstruction. Neuroimage 9:179–194. CrossRef Medline

Damoiseaux JS, Prater KE, Miller BL, Greicius MD (2012) Functional connectivity tracks clinical deterioration in Alzheimer's disease. Neurobiol Aging 33:828–830. CrossRef Medline

Desikan RS, Ségonne F, Fischl B, Quinn BT, Dickerson BC, Blacker D, Buckner RL, Dale AM, Maguire RP, Hyman BT, Albert MS, Killiany RJ (2006) An automated labeling system for subdividing the human cerebral cortex on MRI scans into gyral based regions of interest. Neuroimage 31:968–980. CrossRef Medline

Filippini N, MacIntosh BJ, Hough MG, Goodwin GM, Frisoni GB, Smith SM, Matthews PM, Beckmann CF, Mackay CE (2009) Distinct patterns of brain activity in young carriers of the APOE-epsilon4 allele. Proc Natl Acad Sci U S A 106:7209–7214. CrossRef Medline

Fischl B, Salat DH, Busa E, Albert M, Dieterich M, Haselgrove C, van der Kouwe A, Killiany R, Kennedy D, Klaveness S, Montillo A, Makris N, Rosen B, Dale AM (2002) Whole brain segmentation: automated labeling of neuroanatomical structures in the human brain. Neuron 33:341–355. CrossRef Medline

Folstein MF, Folstein SE, McHugh PR (1975) "Mini-mental state." A practical method for grading the cognitive state of patients for the clinician. J Psychiatr Res 12:189–198. CrossRef Medline

Freire L, Mangin JF (2001) Motion correction algorithms may create spurious brain activations in the absence of subject motion. Neuroimage 14:709–722. CrossRef Medline

Greve DN, Salat DH, Bowen SL, Izquierdo-Garcia D, Schultz AP, Catana C, Becker JA, Svarer C, Knudsen GM, Sperling RA, Johnson KA (2016) Different partial volume correction methods lead to different conclusions: an (18)F-FDG PET study of aging. Neuroimage 132:334–343. CrossRef Medline

Hallquist MN, Hwang K, Luna B (2013) The nuisance of nuisance regression: spectral misspecification in a common approach to resting-state fMRI preprocessing reintroduces noise and obscures functional connectivity. Neuroimage 82:208–225. CrossRef Medline

Hardy JA, Higgins GA (1992) Alzheimer's disease: the amyloid cascade hypothesis. Science 256:184–185. CrossRef Medline

Hedden T, Van Dijk KR, Becker JA, Mehta A, Sperling RA, Johnson KA, Buckner RL (2009) Disruption of functional connectivity in clinically normal older adults harboring amyloid burden. J Neurosci 29:12686–12694. CrossRef Medline

Huijbers W, Mormino EC, Schultz AP, Wigman S, Ward AM, Larvie M, Amariglio RE, Marshall GA, Rentz DM, Johnson KA, Sperling RA (2015) Amyloid-$\beta$ deposition in mild cognitive impairment is associated with increased hippocampal activity, atrophy and clinical progression. Brain 138:1023–1035. CrossRef Medline

Jack CR Jr, Wiste HJ, Weigand SD, Knopman DS, Lowe V, Vemuri P, Mielke MM, Jones DT, Senjem ML, Gunter JL, Gregg BE, Pankratz VS, Petersen RC (2013) Amyloid-first and neurodegeneration-first profiles characterize incident amyloid PET positivity. Neurology 81:1732–1740. CrossRef Medline

Jack CR Jr, Bennett DA, Blennow K, Carrillo MC, Feldman HH, Frisoni GB, Hampel H, Jagust WJ, Johnson KA, Knopman DS, Petersen RC, Scheltens P, Sperling RA, Dubois B (2016) A/T/N: an unbiased descriptive classification scheme for Alzheimer disease biomarkers. Neurology 87:539–547. CrossRef Medline

Johnson KA, Schultz AP, Betensky RA, Becker JA, Sepulcre J, Rentz D, Mormino E, Chhatwal J, Amariglio R, Papp K, Marshall G, Albers M, Mauro S, Pepin L, Alverio J, Judge K, Philiossaint M, Shoup T, Yokell D, Dickerson B, et al (2016) Tau positron emission tomographic imaging in aging and early Alzheimer disease. Ann Neurol 79:110–119. CrossRef Medline

Jones DT, Knopman DS, Gunter JL, Graff-Radford J, Vemuri P, Boeve BF, Petersen RC, Weiner MW, Jack CR Jr, Jack CR Jr (2016) Cascading network failure across the Alzheimer's disease spectrum. Brain 139:547–562. CrossRef Medline

Khambhati AN, Davis KA, Oommen BS, Chen SH, Lucas TH, Litt B, Bassett, DS (2015) Dynamic network drivers of seizure generation, propagation and termination in human neocortical epilepsy. PLoS Comput Biol 11:e1004608. CrossRef Medline

Labbe C, Koepp M, Ashburner J, Spinks T, Richardson M, Duncan J, Cunningham V (1998) Absolute PET quantification with correction for partial volume effects within cerebral structures. In: Quantitative functional brain imaging with positron emission tomography (Carson RE, Daube-Witherspoon ME, Herscovitch P, eds), pp 59–66. San Diego: Academic.

La Corte V, Sperduti M, Malherbe C, Vialatte F, Lion S, Gallarda T, Oppenheim C, Piolino P (2016) Cognitive decline and reorganization of functional connectivity in healthy aging: the pivotal role of the salience network in the prediction of age and cognitive performances. Front Aging Neurosci 8:204. CrossRef Medline

Lim HK, Nebes R, Snitz B, Cohen A, Mathis C, Price J, Weissfeld L, Klunk W, Aizenstein HJ (2014) Regional amyloid burden and intrinsic connectivity networks in cognitively normal elderly subjects. Brain 137:3327–3338. CrossRef Medline

Logan J, Fowler JS, Volkow ND, Wolf AP, Dewey SL, Schlyer DJ, MacGregor RR, Hitzemann R, Bendriem B, Gatley SJ (1990) Graphical analysis of reversible radioligand binding from time-activity measurements applied to [N-11C-methyl]-cocaine PET studies in human subjects. J Cereb Blood Flow Metab 10:740–747. CrossRef Medline

Machulda MM, Jones DT, Vemuri P, McDade E, Avula R, Przybelski S, Boeve BF, Knopman DS, Petersen RC, Jack CR Jr (2011) Effect of APOE $\varepsilon$4 status on intrinsic network connectivity in cognitively normal elderly subjects. Arch Neurol 68:1131–1136. CrossRef Medline

Miller SL, Celone K, DePeau K, Diamond E, Dickerson BC, Rentz D, Pihlajamäki M, Sperling RA (2008) Age-related memory impairment associated with loss of parietal deactivation but preserved hippocampal activation. Proc Natl Acad Sci U S A 105:2181–2186. CrossRef Medline

Mormino EC, Smiljic A, Hayenga AO, Onami SH, Greicius MD, Rabinovici GD, Janabi M, Baker SL, Yen IV, Madison CM, Miller BL, Jagust WJ (2011) Relationships between $\beta$-amyloid and functional connectivity in different components of the default mode network in aging. Cereb Cortex 21:2399–2407. CrossRef Medline

Mormino EC, Betensky RA, Hedden T, Schultz AP, Ward A, Huijbers W, Rentz DM, Johnson KA, Sperling RA (2014a) Amyloid and APOE $\varepsilon$4 interact to influence short-term decline in preclinical Alzheimer disease. Neurology 82:1760–1767. CrossRef Medline

Mormino EC, Betensky RA, Hedden T, Schultz AP, Amariglio RE, Rentz DM, Johnson KA, Sperling RA (2014b) Synergistic effect of $\beta$-amyloid and neurodegeneration on cognitive decline in clinically normal individuals. JAMA Neurol 71:1379–1385. CrossRef Medline

Morris JC (1993) The Clinical Dementia Rating (CDR): current version and scoring rules. Neurology 43:2412–2414. Medline

Oh H, Steffener J, Razlighi QR, Habeck C, Liu D, Gazes Y, Janicki S, Stern Y (2015) A$\beta$-related hyperactivation in frontoparietal control regions in cognitively normal elderly. Neurobiol Aging 36:3247–3254. CrossRef Medline

Oh H, Steffener J, Razlighi QR, Habeck C, Stern Y (2016) $\beta$-Amyloid deposition is associated with decreased right prefrontal activation during task switching among cognitively normal elderly. J Neurosci 36:1962–1970. CrossRef Medline

Ossenkoppele R, Schonhaut DR, Schöll M, Lockhart SN, Ayakta N, Baker SL, O'Neil JP, Janabi M, Lazaris A, Cantwell A, Vogel J, Santos M, Miller ZA, Bettcher BM, Vossel KA, Kramer JH, Gorno-Tempini ML, Miller BL, Jagust WJ, Rabinovici GD (2016) Tau PET patterns mirror clinical and neuroanatomical variability in Alzheimer's disease. Brain 139:1551–1567. CrossRef Medline

Palop JJ, Mucke L (2009) Epilepsy and cognitive impairments in Alzheimer disease. Arch Neurol 66:435–440. CrossRef Medline

Petrella JR, Sheldon FC, Prince SE, Calhoun VD, Doraiswamy PM (2011) Default mode network connectivity in stable vs progressive mild cognitive impairment. Neurology 76:511–517. CrossRef Medline

Rousset OG, Ma Y, Evans AC (1998) Correction for partial volume effects in PET: principle and validation. J Nucl Med 39:904–911. Medline

Schöll M, Lockhart SN, Schonhaut DR, O'Neil JP, Janabi M, Ossenkoppele R, Baker SL, Vogel JW, Faria J, Schwimmer HD, Rabinovici GD, Jagust WJ (2016) PET imaging of tau deposition in the aging human brain. Neuron 89:971–982. CrossRef Medline

Schultz AP, Chhatwal JP, Huijbers W, Hedden T, van Dijk KR, McLaren DG, Ward AM, Wigman S, Sperling RA (2014) Template based rotation: a method for functional connectivity analysis with a priori templates. Neuroimage 102:620–636. CrossRef Medline

Sepulcre J, Schultz AP, Sabuncu MR, Gomez Isla T, Chhatwal JP, Becker A, Sperling R, Johnson KA (2016) *In vivo* tau, amyloid, and gray matter profiles in the aging brain. J Neurosci 36:7364–7374. CrossRef Medline

Shaw EE, Schultz AP, Sperling RA, Hedden T (2015) Functional connectivity in multiple cortical networks is associated with performance across cognitive domains in older adults. Brain Connect 5:505–516. CrossRef Medline

Sheline YI, Raichle ME, Snyder AZ, Morris JC, Head D, Wang S, Mintun MA (2010a) Amyloid plaques disrupt resting state default mode network connectivity in cognitively normal elderly. Biol Psychiatry 67:584–587. CrossRef Medline

Sheline YI, Morris JC, Snyder AZ, Price JL, Yan Z, D'Angelo G, Liu C, Dixit S, Benzinger T, Fagan A, Goate A, Mintun MA (2010b) APOE4 allele disrupts resting state fMRI connectivity in the absence of amyloid plaques or decreased CSF A$\beta$42. J Neurosci 30:17035–17040. CrossRef Medline

Shoup TM, Yokell DL, Rice PA, Jackson RN, Livni E, Johnson KA, Brady TJ, Vasdev N (2013) A concise radiosynthesis of the tau radiopharmaceutical, [(18) F]T807. J Labelled Comp Radiopharm 56:736–740. CrossRef Medline

Sperling RA, LaViolette PS, O'Keefe K, O'Brien J, Rentz DM, Pihlajamaki M, Marshall G, Hyman BT, Selkoe DJ, Hedden T, Buckner RL, Becker JA, Johnson KA (2009) Amyloid deposition is associated with impaired default network function in older persons without dementia. Neuron 63:178–188. CrossRef Medline

Sperling RA, Hedden T, Dickerson BC, Pihlajamaki MM, Vannini P, LaViolette PS, et al (2010) Functional alterations in memory networks in early Alzheimer's disease. Neuromol Med 12:27–43. CrossRef Medline

Sperling RA, Aisen PS, Beckett LA, Bennett DA, Craft S, Fagan AM, Iwatsubo T, Jack CR Jr, Kaye J, Montine TJ, Park DC, Reiman EM, Rowe CC, Siemers E, Stern Y, Yaffe K, Carrillo MC, Thies B, Morrison-Bogorad M, Wagster MV, et al (2011) Toward defining the preclinical stages of Alzheimer's disease: recommendations from the National Institute on Aging-Alzheimer's Association workgroups on diagnostic guidelines for Alzheimer's disease. Alzheimers Dement (N Y) 7:280–292. CrossRef Medline

Sperling R, Mormino E, Johnson K (2014) The evolution of preclinical Alzheimer's disease: implications for prevention trials. Neuron 84:608–622. CrossRef Medline

Van Dijk KR, Hedden T, Venkataraman A, Evans KC, Lazar SW, Buckner RL (2010) Intrinsic functional connectivity as a tool for human connectomics: theory, properties, and optimization. J Neurophysiol 103:297–321. CrossRef Medline

Villemagne VL, Fodero-Tavoletti MT, Masters CL, Rowe CC (2015) Tau imaging: early progress and future directions. Lancet Neurol 14:114–124. CrossRef Medline

Vincent JL, Snyder AZ, Fox MD, Shannon BJ, Andrews JR, Raichle ME, Buckner RL (2006) Coherent spontaneous activity identifies a hippocampal-parietal memory network. J Neurophysiol 96:3517–3531. CrossRef Medline

Vos SJ, Verhey F, Frölich L, Kornhuber J, Wiltfang J, Maier W, Peters O, Rüther E, Nobili F, Morbelli S, Frisoni GB, Drzezga A, Didic M, van Berckel BN, Simmons A, Soininen H, Kłoszewska I, Mecocci P, Tsolaki M, Vellas B, et al (2015) Prevalence and prognosis of Alzheimer's disease at the mild cognitive impairment stage. Brain 138:1327–1338. CrossRef Medline

Vossel KA, Beagle AJ, Rabinovici GD, Shu H, Lee SE, Naasan G, Hegde M, Cornes SB, Henry ML, Nelson AB, Seeley WW, Geschwind MD, Gorno-Tempini ML, Shih T, Kirsch HE, Garcia PA, Miller BL, Mucke L (2013) Seizures and epileptiform activity in the early stages of Alzheimer disease. JAMA Neurol 70:1158–1166. CrossRef Medline

Wang K, Liang M, Wang L, Tian L, Zhang X, Li K, Jiang T (2007) Altered functional connectivity in early Alzheimer's disease: a resting-state fMRI study. Hum Brain Mapp 28:967–978. CrossRef Medline

Wang L, Brier MR, Snyder AZ, Thomas JB, Fagan AM, Xiong C, Benzinger TL, Holtzman DM, Morris JC, Ances BM (2013) Cerebrospinal fluid A$\beta$42, phosphorylated Tau181, and resting-state functional connectivity. JAMA Neurol 70:1242–1248. CrossRef Medline

Ward AM, Schultz AP, Huijbers W, Van Dijk KR, Hedden T, Sperling RA (2014) The parahippocampal gyrus links the default-mode cortical network with the medial temporal lobe memory system. Hum Brain Mapp 35:1061–1073. CrossRef Medline

Ward AM, Mormino EC, Huijbers W, Schultz AP, Hedden T, Sperling RA (2015) Relationships between default-mode network connectivity, medial temporal lobe structure, and age-related memory deficits. Neurobiol Aging 36:265–272. CrossRef Medline

Wechsler D (1987) Wechsler Memory Scale-Revised. San Antonio, TX: Psychological Corp.

Westlye ET, Lundervold A, Rootwelt H, Lundervold AJ, Westlye LT (2011) Increased hippocampal default mode synchronization during rest in middle-aged and elderly APOE 4 carriers: relationships with memory performance. J Neurosci 31:7775–7783. CrossRef Medline

Whitfield-Gabrieli S, Thermenos HW, Milanovic S, Tsuang MT, Faraone SV, McCarley RW, et al (2009) Hyperactivity and hyperconnectivity of the default network in schizophrenia and in first-degree relatives of persons with schizophrenia. Proc Natl Acad Sci U S A, 106:1279–1284. CrossRef Medline

Wu JW, Hussaini SA, Bastille IM, Rodriguez GA, Mrejeru A, Rilett K, Sanders DW, Cook C, Fu H, Boonen RA, Herman M, Nahmani E, Emrani S, Figueroa YH, Diamond MI, Clelland CL, Wray S, Duff KE (2016) Neuronal activity enhances tau propagation and tau pathology in vivo. Nat Neurosci 19:1085–1092. CrossRef Medline

Yesavage JA, Brink TL, Rose TL, Lum O, Huang V, Adey M, Leirer VO (1982) Development and validation of a geriatric depression screening scale: a preliminary report. J Psychiatr Res 17:37–49. CrossRef Medline